Computational studies of two unconventional approximation schemes for mechanical system responses

A project report submitted in fulfilment of the requirements

for the degree of Master of Technology

by

Vaibhav Pratap Singh

(16807768)

to the

DEPARTMENT OF MECHANICAL ENGINEERING

INDIAN INSTITUTE OF TECHNOLOGY KANPUR

July 2021

Certificate

It is certified that the work contained in this project entitled **Computational studies of two unconventional approximation schemes for mechanical system responses** by **Vaibhav Pratap Singh** has been carried out under my supervision and that it has not been submitted elsewhere for a degree.

Prof. Anindya Chatterjee

Professor

Department of Mechanical Engineering

Indian Institute of Technology Kanpur

July 2021

Declaration

This is to certify that the project report titled **Computational studies of two unconventional approximation schemes for mechanical system responses** has been authored by me. It presents the research conducted by me under the supervision of Prof. Anindya Chatterjee

To the best of my knowledge, it is an original work, both in terms of research content and narrative, and has not been submitted elsewhere, in part or in full, for a degree. Due credit has been attributed to the relevant state-of-the-art and collaborations (if any) with appropriate citations and acknowledgements, in line with established norms and practices.

Vaibhav Pratap Singh

BT-MT (Dual Degree)

Department of Mechanical Engineering

Indian Institute of Technology, Kanpur

Kanpur - 208016

Abstract

Name of the student: **Vaibhav Pratap Singh** Roll No: **16807768**

Degree for which submitted: **M.Tech.** Department: **Mechanical Engineering**

Project title: **Computational studies of two unconventional approximation schemes for mechanical system responses**

Project supervisor: **Prof. Anindya Chatterjee**

Month and year of project submission: **July 2021**

Unconventional approximation techniques for two different mechanical system responses are developed in this study. Many systems exhibit decaying responses, and an unorthodox approach is used here to approximate them. A delayed dynamical system is constructed using convolution integrals such that one possible set of responses includes the desired response characteristics. Combination of discrete and distributed feedbacks are found, constructing the delayed differential equation. Roots of the established delayed differential equation are used as a basis to fit the function in question using an infinity norm solver. With increase in terms, the fit obtained is excellent for certain functions. The second system involves planar pushing, one of the basic manipulation primitives that a robot can use for mechanical tasks. For robot motion planning, a simple mapping from load to motion is used. This mapping uses an approximated limit load surface. we propose a new approximation which uses a small number of symmetrical 3×3 matrices along with fractional powers of simple quadratic forms. Fitting these 3×3 matrices is easy with simple optimization algorithms. Several numerical examples show that with 2 or 3 such fitted matrices, the fit obtained is excellent. The new method of approximating limit load surfaces presents a significant useful generalization of the popular but somewhat inaccurate ellipsoid approach.

Acknowledgements

I would extend my sincerest gratitude to my project advisor Prof. Anindya Chatterjee for guiding and supporting me in the right direction. I would also like to thank Sankalp Tiwari and Devesh Jha for fruitful discussions and multiple insights on the problem statement and providing me relevant information to do the work.

I would like to thank my parents and brother for supporting and providing me encouragement throughout my years of study. It would have been difficult to complete the project without their assistance.

I'd also like to thank my batchmates Shubham, Manu, Gaurav, Akshay, Umesh, and Akash for their help and encouragement along this journey.

Vaibhav Pratap Singh
Department of Mechanical Engineering
IIT Kanpur

Contents

List of Figures

Abbreviations

LS	**L**imit **S**urface
COR	**C**enter **O**f **R**otation
DDE	**D**elayed **D**ifferential **E**quation

Symbols

α	Alpha
P	Load vector
v	motion vector
F	Force
$\hat{v}$	Approximated velocity
$\hat{f}$	Approximated force
f_s	Scaled force

Dedicated to my mother
Mrs. Nivedita Chauhan

Chapter 1

Introduction

This study examines two mechanical systems first involving decaying functions and the second involving planar body sliding. On both areas, the study proposes an unconventional approximation technique. In this way the report has a two part structure to it. In Chapter 2, we use the hockey stick function as an example to present an approximation strategy for decaying functions. We establish our method and analyse the approximation. In Chapter 3, we approximate certain closed convex surfaces known as limit surfaces using our proposed formulation. We also study what these limit surfaces are, how they are generated, and why they must be precisely approximated. We examine how our formulation works with increasing terms and varied objective functions, comparing it to past work.

The following is an overview of the two problems being investigated. The subsequent chapters delve deeper into these topics. This report comes to a close with concluding remarks on both the themes.

1.1 Approximation for decaying functions

Some systems have a scalar response that starts at a high value and then decays to low values with the passage of time. The usual approach is to fit the response using a linear combination of decaying exponentials. When the number of terms in the sum becomes large, then choosing the exponential rates (which can be complex, i.e., with oscillating components) can be difficult. For instance, fitting exponential rates along with the coefficients would give an exponential equation which would be ill-conditioned when solved in a least square sense. If posed as an optimization problem, there are many local minima

and finding a good solution is not guaranteed in advance for arbitrary numbers of terms in the approximation. Here we take an indirect approach to the problem, by constructing a delayed dynamical system whose possible set of free responses includes the specific function of time in question.

1.2 Approximations for limit surfaces

The second problem studied in this work involves frictional slipping motions of flat or planar objects subjected to forces and moments. Consider a rigid body sliding on a planar surface. The only interaction of this body with the surface are the frictional forces, which are studied. The contact normal force or pressure is known. If the motion is known, then computing the required loads is straightforward (although it includes evaluation of integrals). Conversely, if the load direction is known, then predicting the initial motion direction is more difficult because it requires solution of nonlinear equations which involve evaluation of integrals. In robotics, there is interest in simple descriptions of force to velocity mapping and vice versa. Simple models based on ellipsoids and polynomials have been developed to investigate this in the past. We attempt to develop a new model for this problem that is more accurate in terms of estimating velocity and forces.

This may appear to be a simple modelling problem, but its applications in the area of robotic manipulation are critical. So far, robots have been used to pick and place items, but we want to utilise them to manipulate the surroundings. This is where these models come into play, they are a vital part in the decision-making process.

Chapter 2

Approximation for decaying functions

In this chapter, we propose a scheme to approximate decaying functions as sum of exponentials. The basic idea is to construct a delayed dynamical system such that one of the responses of the system corresponds to the function that is to be approximated. We develop a scheme to setup the aforementioned system using convolution integral and construct a response that closely approximates the target decaying function. Later on we study how the approximation performs with increasing terms and with different functions.

2.1 A dynamical model

We wish to approximate a function $x(t)$ (for $t > 0$) that eventually decays to zero as t increases, using a linear combination of decaying exponentials. We further wish to use the infinity-norm in our approximation. For demonstration of ideas, we use the hockey stick function (Figure 2.1), defined as $x(t) = 1 - t$ for $0 \leq t \leq 1$, and $x(t) = 0$ otherwise. In principle, every linear combination of exponentials is the solution to some linear constant coefficient dynamic system. A fairly general form of the same may be expressed using a convolution integral as follows:

$$\dot{x}(t) = -\int_0^t f(\tau)x(t-\tau)\,dx \tag{2.1}$$

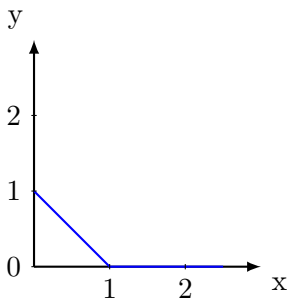

FIGURE 2.1: Hockey stick function

We discretize the above equation and find f using a system of simultaneous linear equations. For the hockey stick function, using 2000 points uniformly spaced on $[0, 6]$, we obtain f. we do the same for 1000 points as well. Results are shown in Figure 2.2.

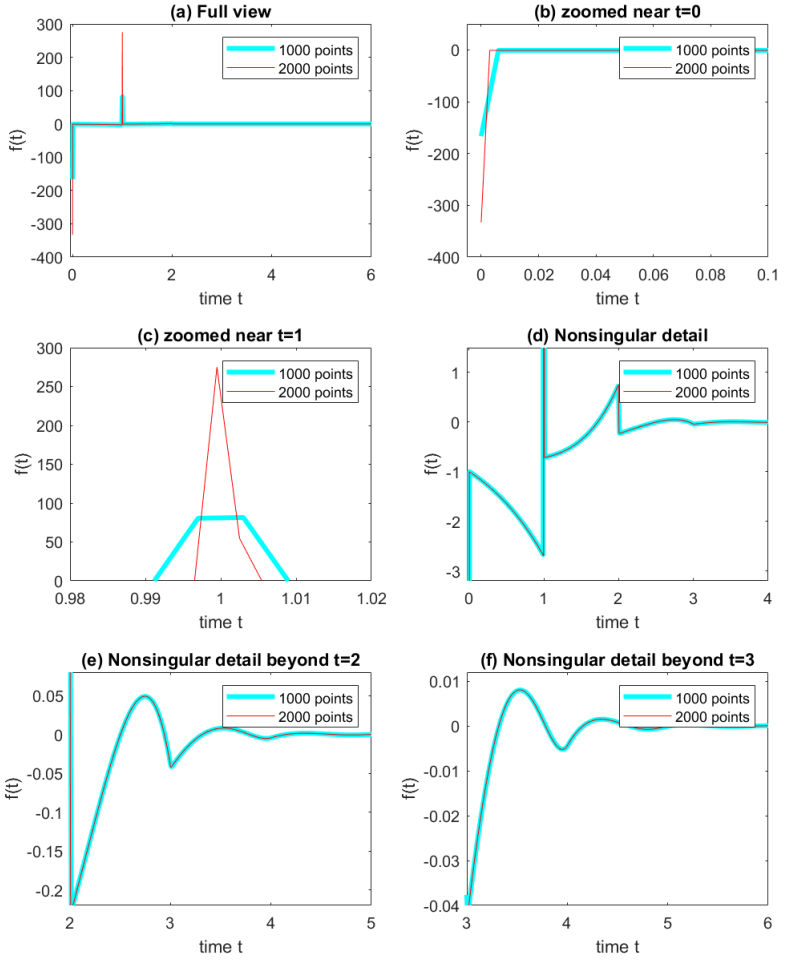

FIGURE 2.2: First view of $f(t)$

2.2 Characterization of f(t)

It is clear from Figure 2.2 that there are Dirac delta functions at $t = 0$ and $t = 1$. Numerical estimates of their strengths suggest both are of unit magnitude. The rest of $f(t)$ can be well approximated by piece-wise polynomials, on the intervals $(0, 1), (1, 2), (2, 3)$ and soon. We choose to ignore the nonzero values of f beyond some large enough t (6 in our case). Six such polynomial plots (each of fifth order) are shown in Figure 2.3 (thick cyan: actual value; thin dotted red: polynomial fit).

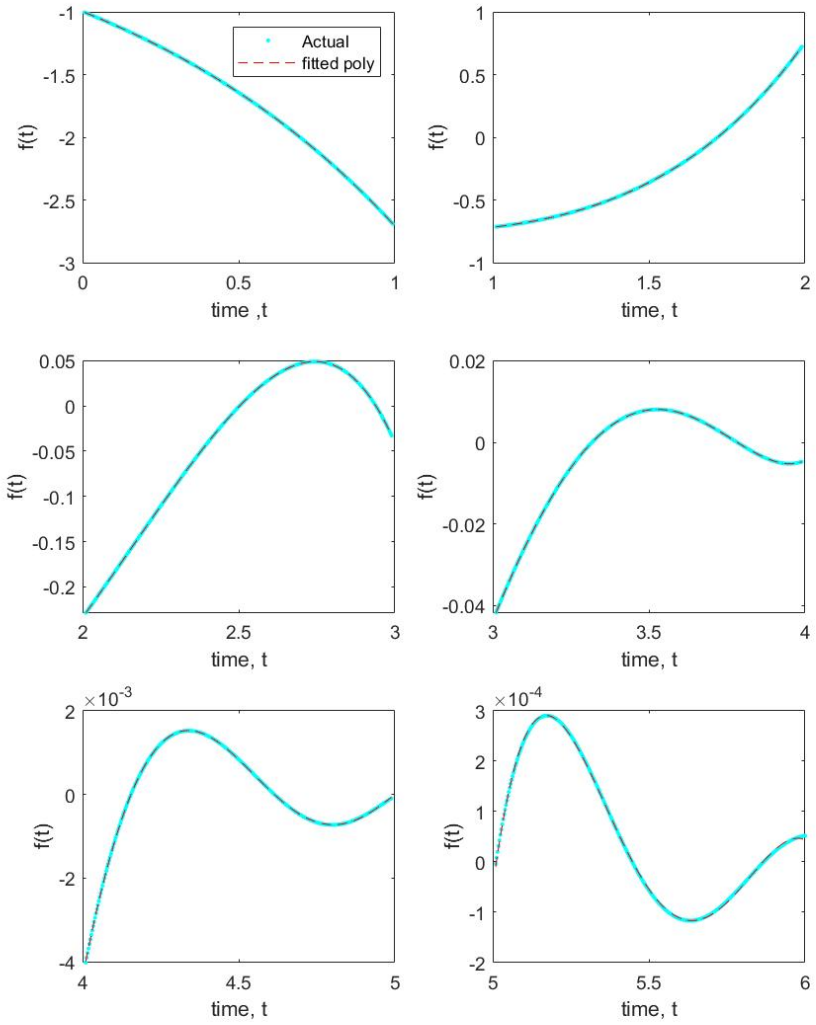

FIGURE 2.3: Piecewise polynomial approximation for $f(t)$

The following are the polynomials that are used to approximate the function over the interval $[0, 6]$. $p_1(t)$ valid for $[0, 1]$ and so on.

$$\begin{aligned}
p_1(t) &= -0.0137t^5 - 0.0345t^4 - 0.0345t^3 - 0.0345t^2 - 0.03451t - 0.9970 \\
p_2(t) &= 0.0657t^5 - 0.2321t^4 + 0.6695t^3 - 0.6433t^2 + 0.1583t - 0.7332 \\
p_3(t) &= -0.1230t^5 + 1.1803t^4 - 4.7502t^3 + 10.1286t^2 - 10.9627t + 4.2296 \\
p_4(t) &= 0.1091t^5 - 1.7157t^4 + 10.7465t^3 - 33.6881t^2 + 53.2784t - 34.3779 \\
p_5(t) &= -0.0411t^5 + 0.9092t^4 - 7.9743t^3 + 34.6855t^2 - 74.7489t + 63.7709 \\
p_6(t) &= 0.0010t^5 - 0.0407t^4 + 0.5696t^3 - 3.8203t^2 + 12.4353t - 15.8333
\end{aligned} \tag{2.2}$$

Now we have established our delay differential equation.

2.3 Delay differential equation

Our system is formed by the dirac delta functions leading to discrete delayed feedback, while the rest of f leading to distributed delayed feedback through integrals, given by eqn (2.3).

$$\dot{x}(t) = -x(t) + x(t-1) + \int_0^1 p_1(\tau)x(t-\tau)d\tau + ... + \int_5^6 p_6(\tau)x(t-\tau)d\tau \tag{2.3}$$

The characteristic roots of the above DDE give us a choice of exponential rates to use for the problem of approximating the original function $x(t)$. Lets refer to them as basis1 for the approximation. Now we insert $x(t) = e^{\lambda t}$ in the DDE, carry out the integrations, and obtain the characteristic equation. We solve this equation in Maple. The characteristic equation obtained is

$$\begin{aligned}\lambda^7 = &(\lambda^6+1.991000\lambda^5+2.982700\lambda^4+3.956800\lambda^3+5.060400\lambda^2+4.797600\lambda+9.540000)e^{-1\lambda}\\ &+(-0.132000+0.184800\lambda-0.084100\lambda^5-0.070500\lambda^4-0.034400\lambda^3+0.067200\lambda^2)e^{-6\lambda}\\ &+(5.076000+2.582400\lambda+0.154700\lambda^5+0.154300\lambda^4+0.085000\lambda^3+0.725400\lambda^2)e^{-5\lambda}\\ &+(-18.036000-0.019500\lambda^4-0.935600\lambda^3-4.612800\lambda^2-9.144000\lambda-0.018600\lambda^5)e^{-4\lambda}\\ &+(27.852000-0.016800\lambda^5+0.961700\lambda^4+3.851200\lambda^3+9.787800\lambda^2+14.047200\lambda)e^{-3\lambda}\\ &+(-22.656000-0.991100\lambda^5-2.974400\lambda^4-5.901400\lambda^3-10.030800\lambda^2-11.412000\lambda)e^{-2\lambda}\\ &-1.644000-0.997000\lambda^5-0.995600\lambda^4-0.992000\lambda^3-1.015200\lambda^2-1.000000\lambda^6-0.828000\lambda\end{aligned} \tag{2.4}$$

The above equation is now solved for λ. It is a transcendental equation with infinitely many roots. But the larger roots of such equation usually follow some discernible pattern, so numerically finding several of them is not really difficult (In particular, eventually the real parts change slowly while the imaginary parts are incremented by near-constant amounts.). Newton-Raphson can be used to find the roots of this equation, with some manipulations of initial guesses. We use Maple's *Root-Finding* to solve this equation, the first 62 numerical determined roots are shown the Figure 2.4.

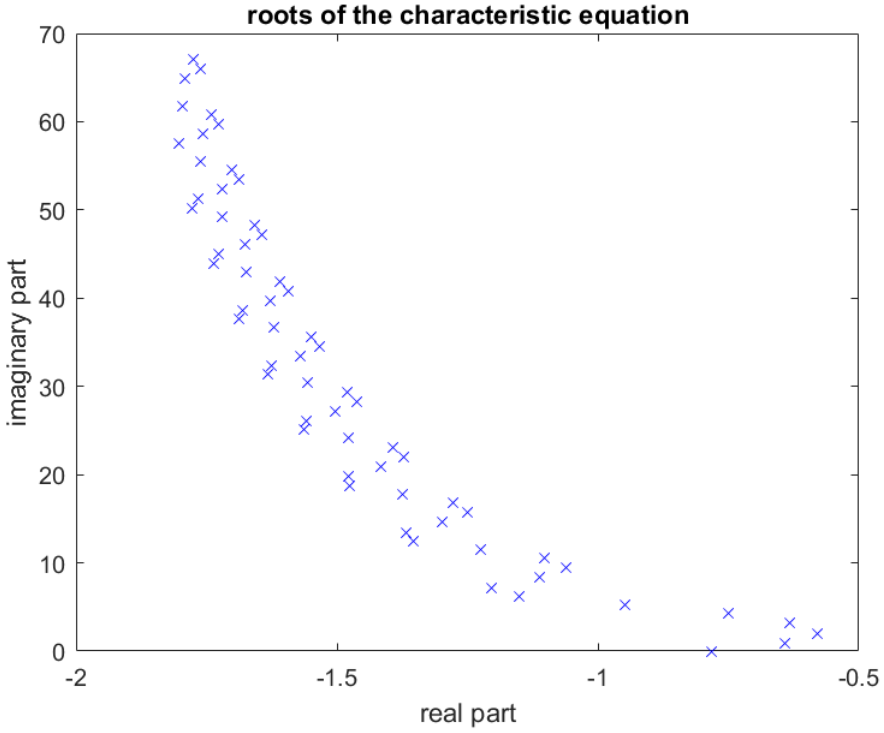

FIGURE 2.4: Roots of characteristic equation

2.4 Least infinity-norm solution

If we have an over determined system $Ax = b$, then the least squares (or minimum-error in 2-norm) solution is easy, and given by MATLAB in response to simply $A\backslash b$. It is less easy, but still standard, to find the solution x that minimizes $\|Ax - b\|_\infty$. We use MATLAB's linprog to do this. Using the infinity-norm minimizing solver, results obtained using 5 roots (i.e., 10 including complex conjugates) are plotted in Figure 2.5. The results obtained using 8 roots are plotted in Figure 2.6. The results obtained using 62 roots are plotted in Figure 2.7.

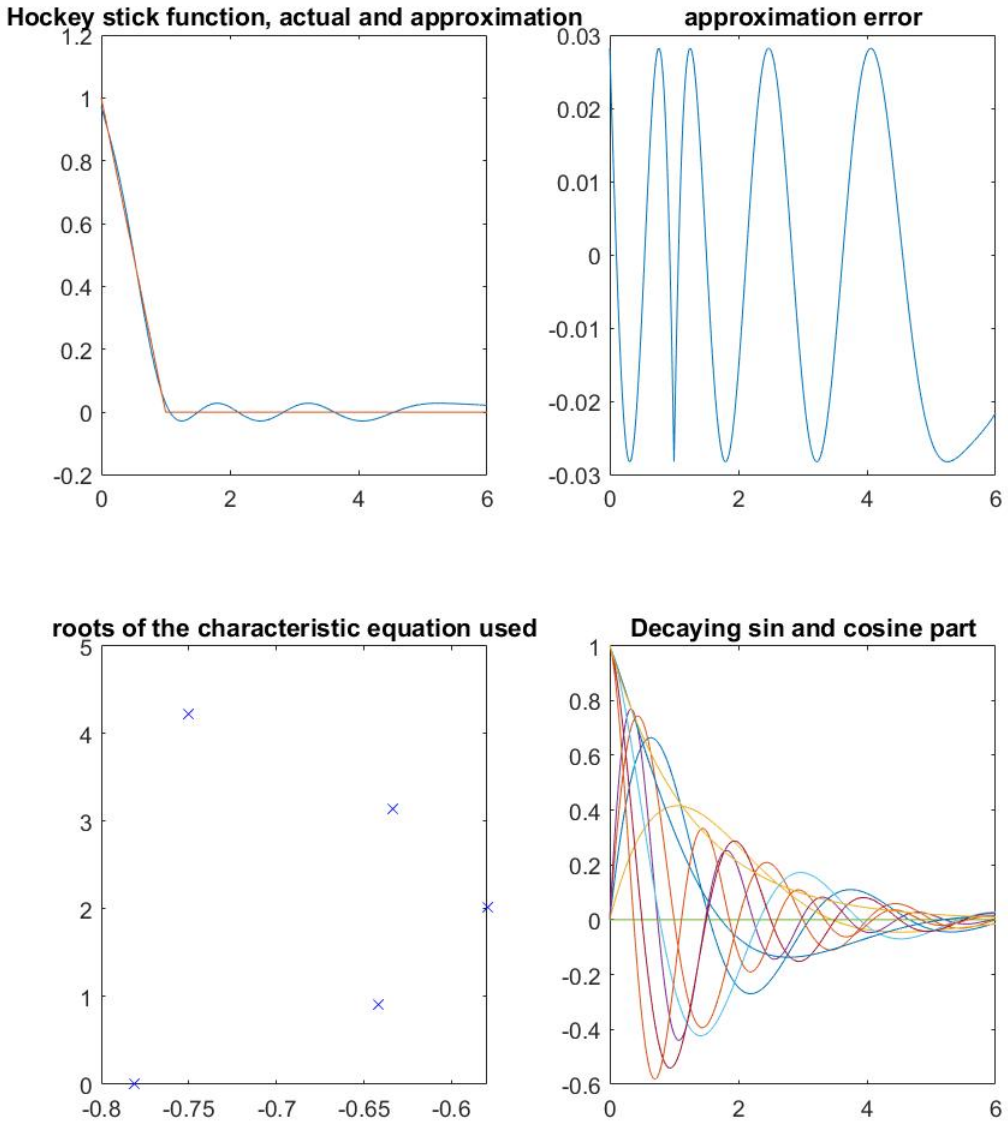

FIGURE 2.5: Approximation obtained using 5×2 roots

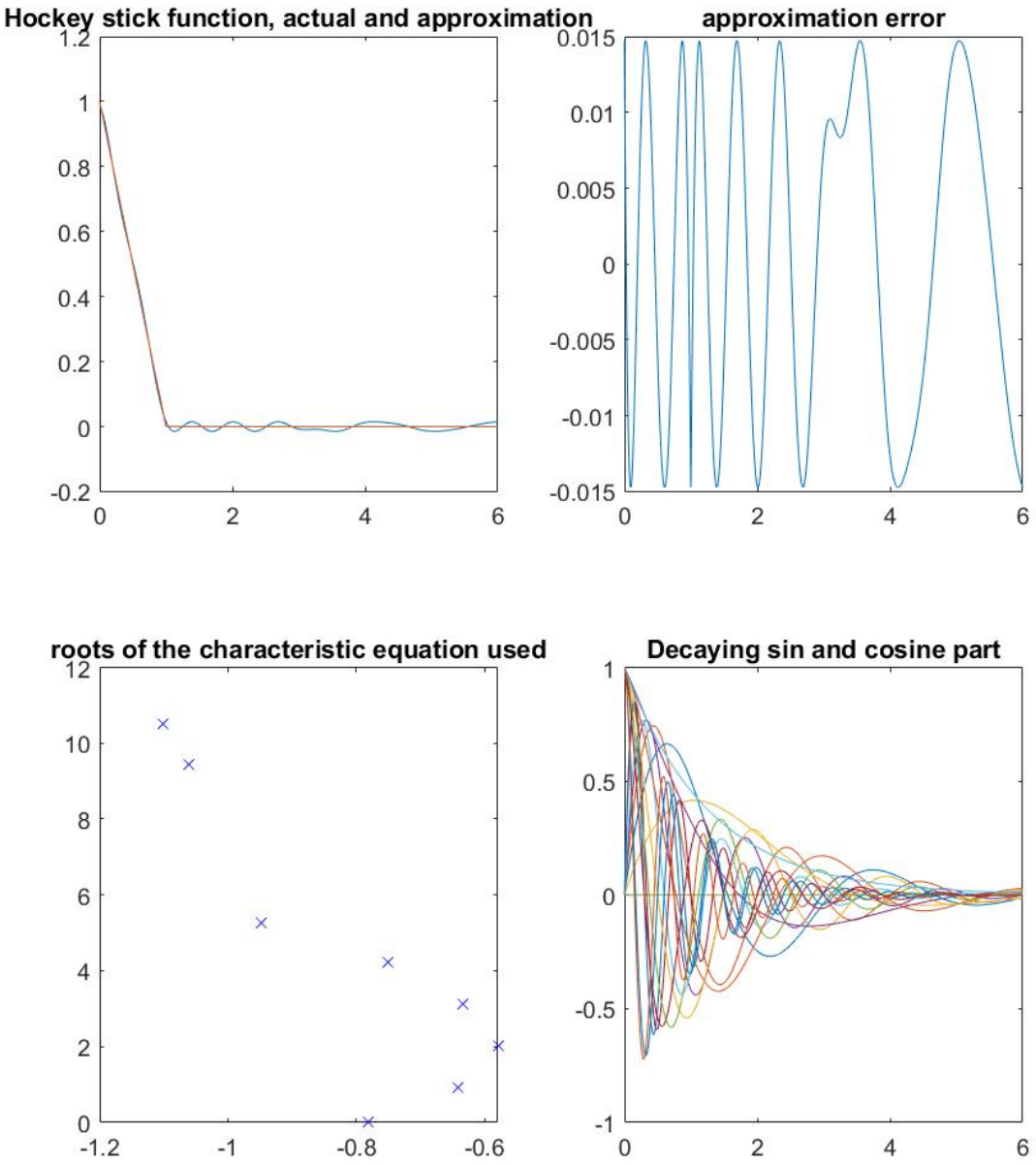

FIGURE 2.6: Approximation obtained using 8×2 roots

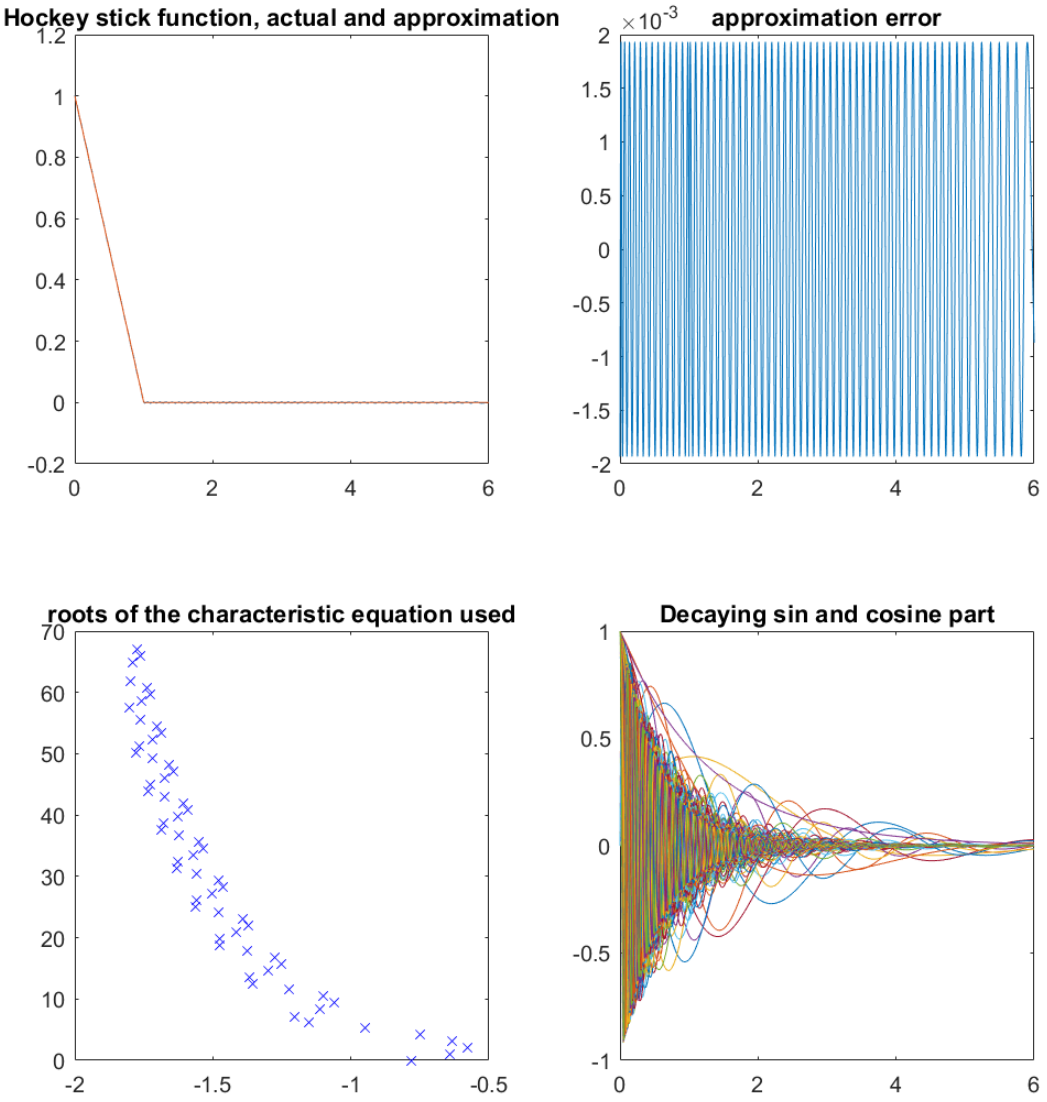

FIGURE 2.7: Approximation obtained using 62×2 roots

The preceding graphs show that as the number of terms increase, the error decreases. Because the roots are complex, oscillations in the error are expected, but the amplitude of these oscillations with increase in terms decrease as the number of terms increase. High frequency sin and cosine parts are introduced into the system as terms increase, contributing to the system's fast varying parts (sharp transition at $t = 1$), giving better results.

2.5 More functions

We repeat the process for a few more functions, yielding a collection of basis. We'll approximate the same functions using these alternative bases to see the changes in approximation and transitions. The functions are approximated from [0,6] and projected until t = 19 to observe the transitions.

To form the basis, we use the following functions. Let us refer to them as f1, f2, and f3 and the basis obtained from them as basis1, basis2, and basis3 respectively. Furthermore, we also use a simple basis (basis0) obtained from the corresponding DDE: $\dot{x}(t) = -0.1x(t-6)$.

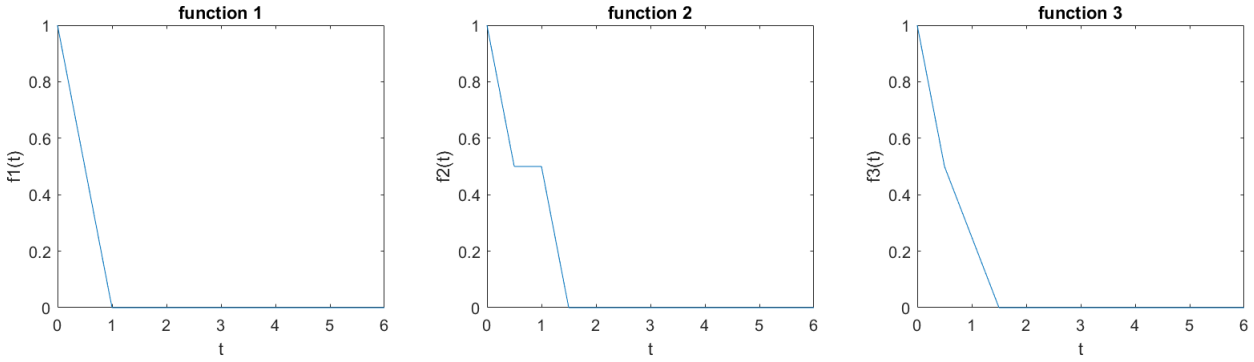

FIGURE 2.8: Function to be approximated

Since f1 is the hockey stick function, calculation for it are carried out in the previous sections, so we will focus on the other two functions. Reiterating the process for the functions, we find four dirac-delta functions in f2 and three in f3 as seen in Figures 2.9 and 2.10 respectively. These contribute to the discrete delayed feedbacks and the rest of the $f(t)$ is approximated by piecewise polynomials on the intervals $(0, 0.5), (0.5, 1)$ and so on, giving the distributed delayed feedback through integrals. Fifth order polynomials are used to approximate these, which are shown in Figure 2.11 and 2.12 for f2 and f3 respectively (cyan: actual value; dotted red: polynomial fit).

Now that polynomials are constructed and dirac-delta functions are known, corresponding DDEs for the respectively functions are established. Figure 2.13 shows the roots obtained after setting up the respective DDEs for the functions.

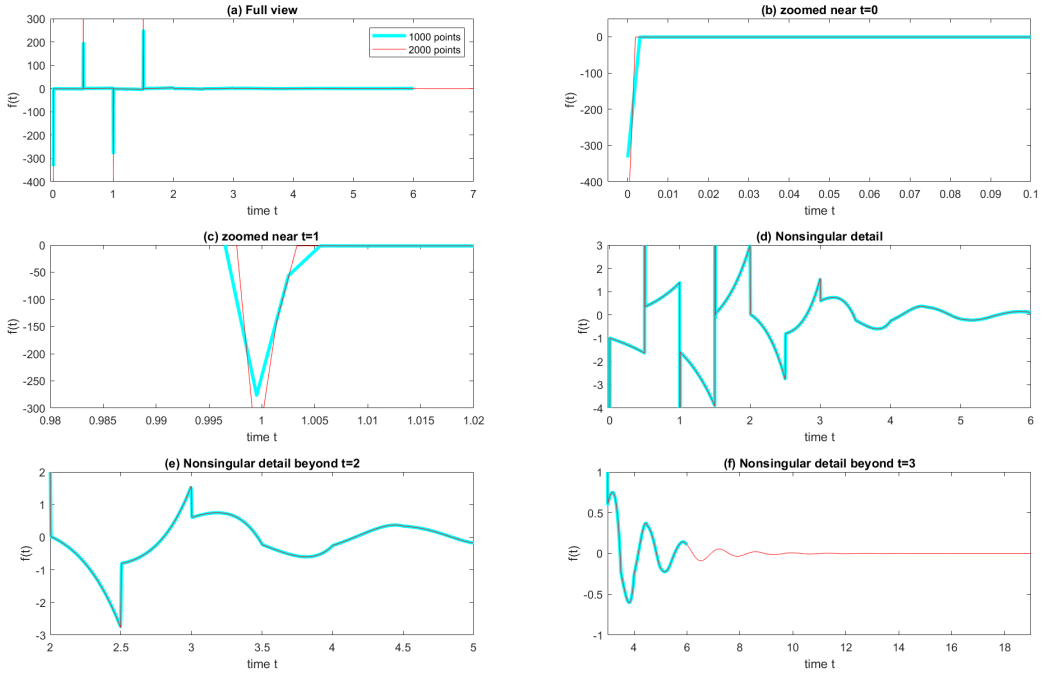

FIGURE 2.9: First view of f for f2

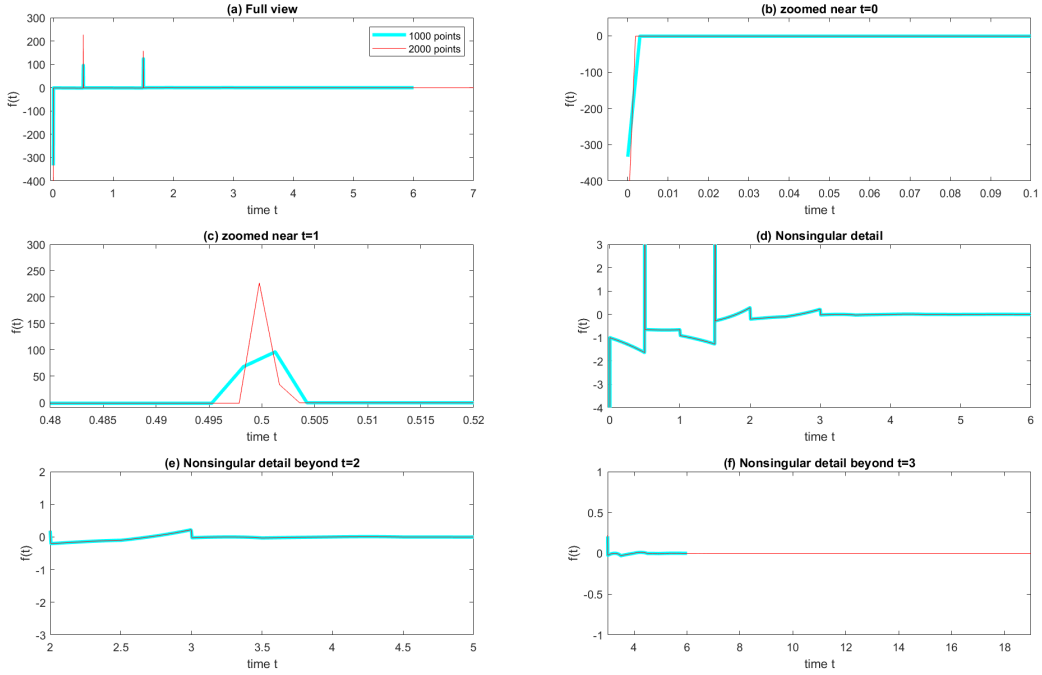

FIGURE 2.10: First view of f for f3

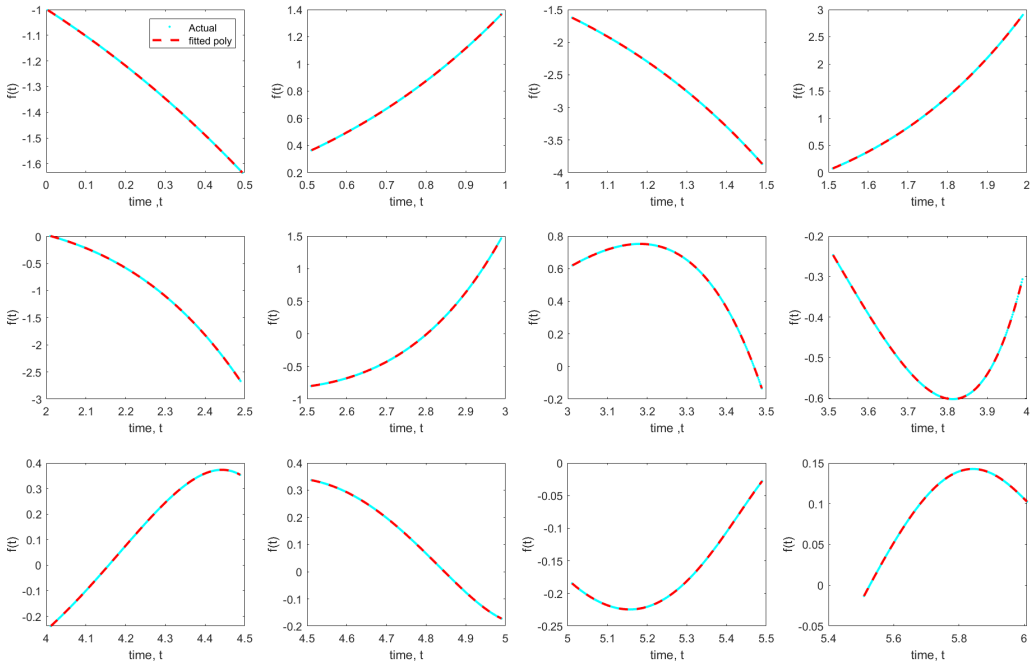

FIGURE 2.11: Piecewise polynomial approximation for f(t) in f2

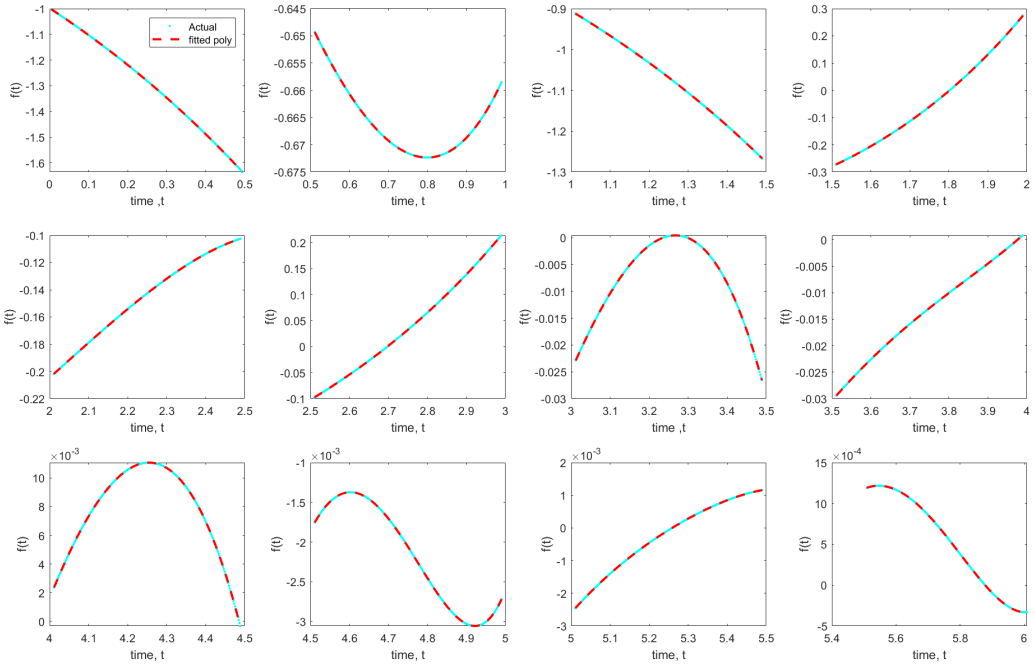

FIGURE 2.12: Piecewise polynomial approximation for f(t) in f3

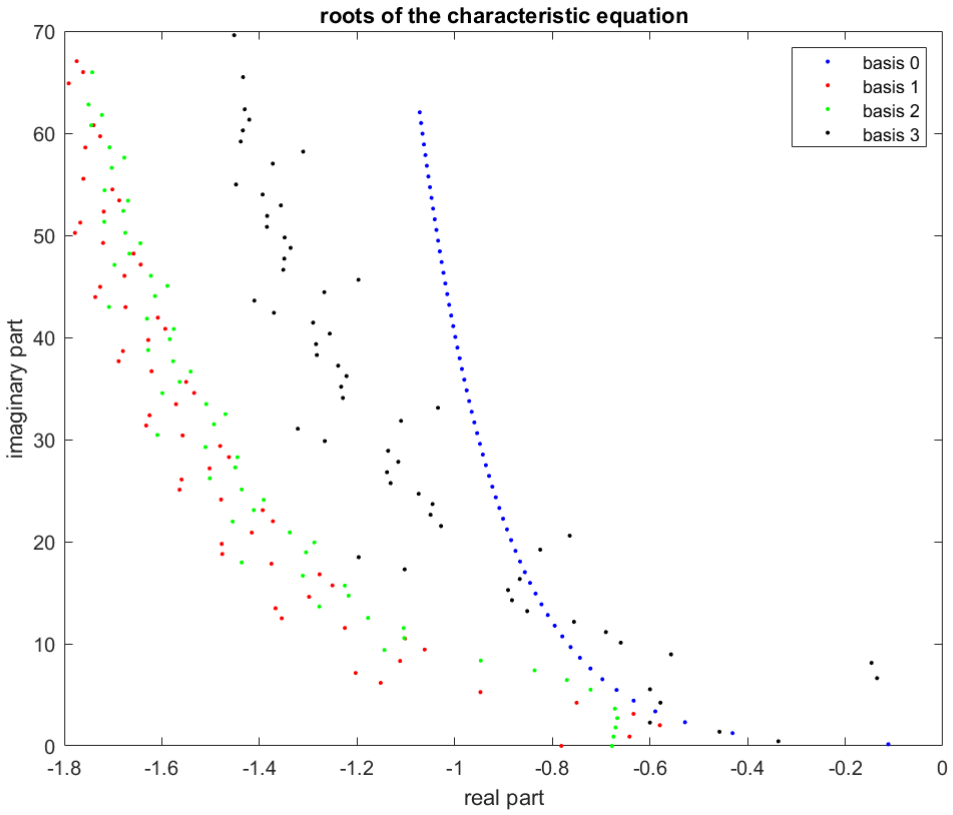

FIGURE 2.13: Roots of respective characteristic equations

We approximate the above functions individually using all of the bases to obtain the best fit and observe the transitions. Figure 2.14 depicts approximation of f1. Figures 2.15 and 2.16 depict the approximation of f2 and f3, respectively.

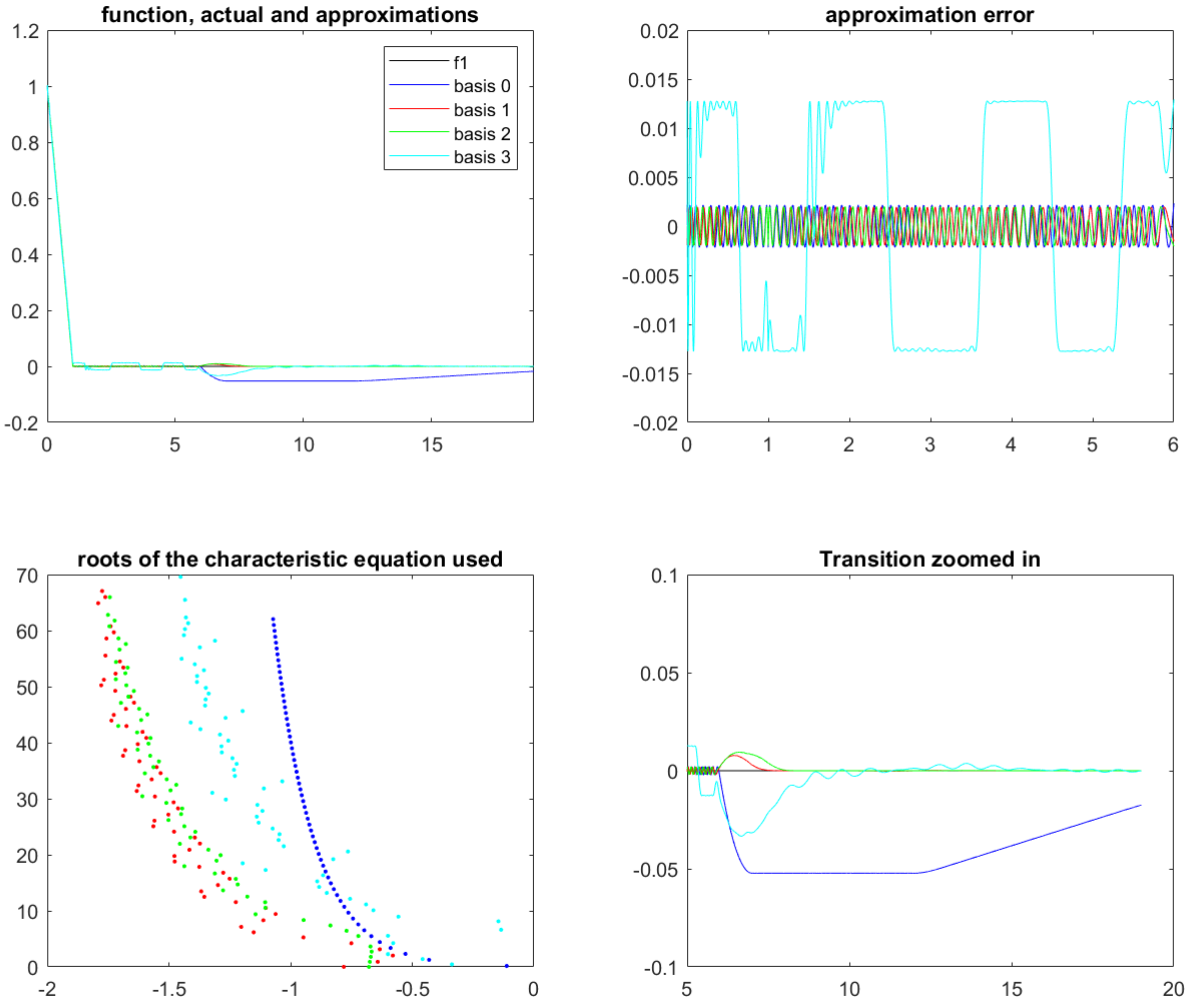

FIGURE 2.14: Approximation of function 1 using different basis

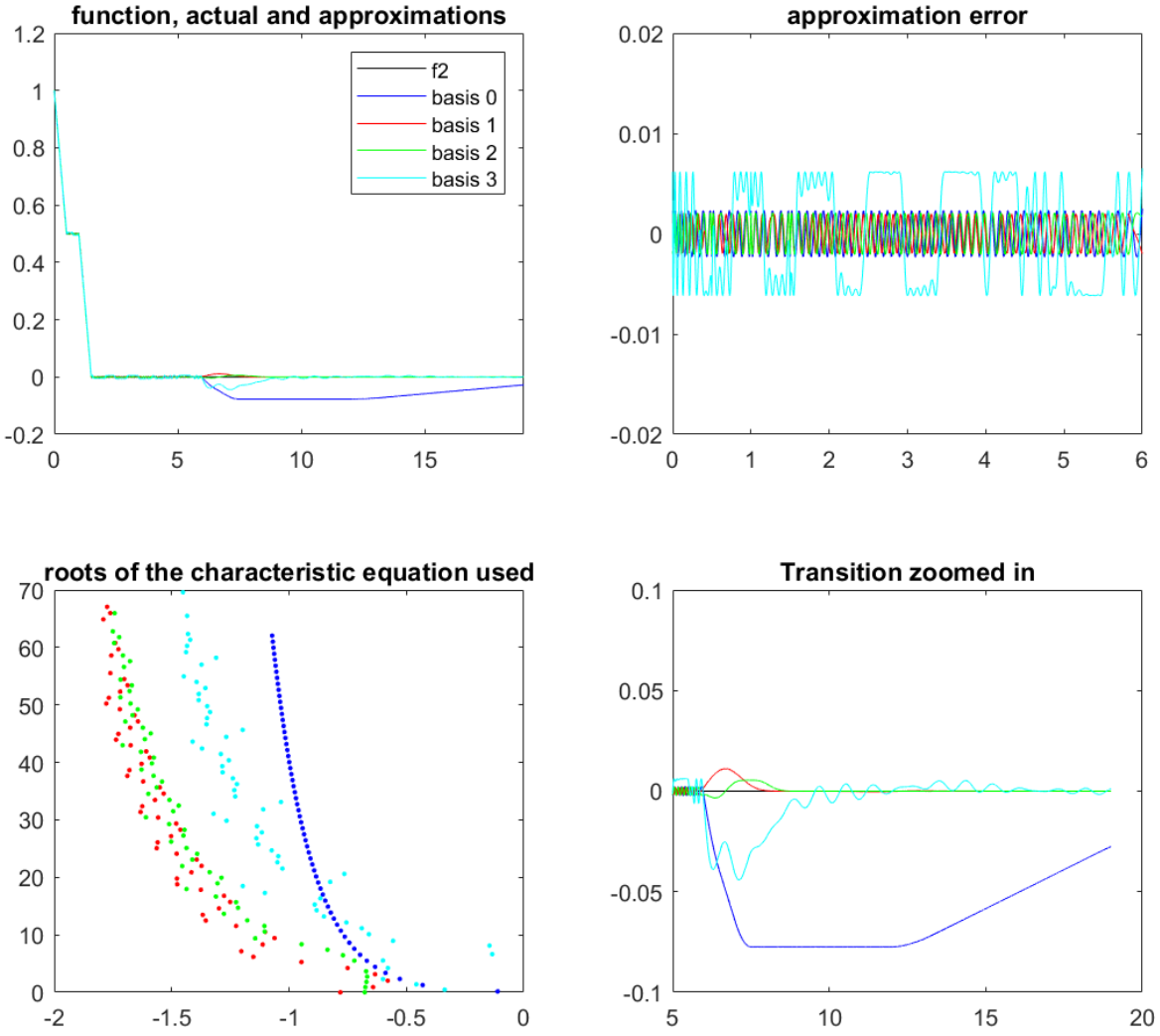

FIGURE 2.15: Approximation of function 2 using different basis

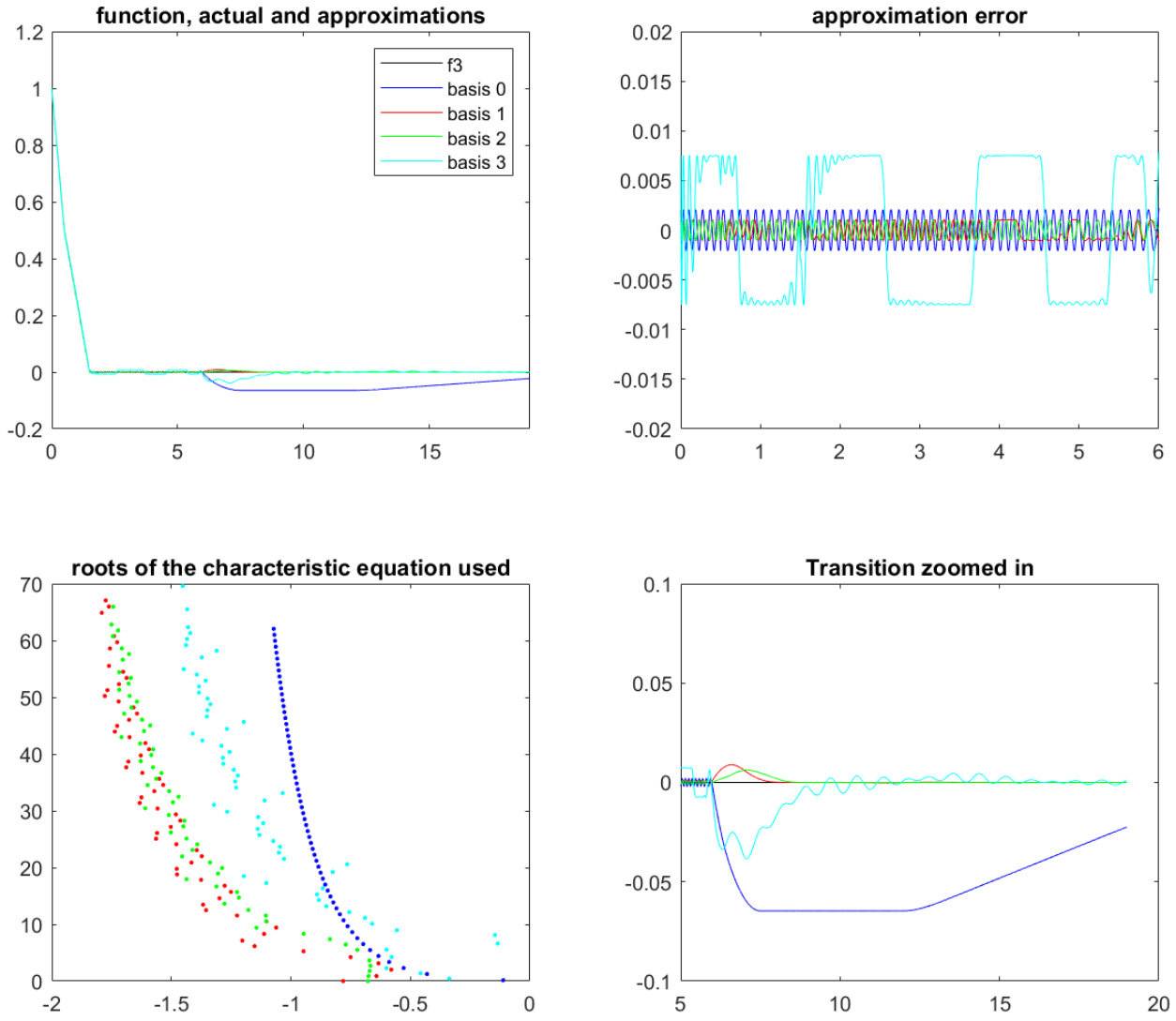

FIGURE 2.16: Approximation of function 3 using different basis

From the above figures it can be noted that the basis3 (cyan) struggles to approximate any of the functions, whereas the other functions give an excellent fit, until the transition. After $t = 6$, the basis0 has a huge dip which eventually decreases whereas the other basis show a small spike that decays eventually. It can be seen that the transition of the functions are almost the same irrespective of the fitted function.

Chapter 3

Approximation for limit surfaces

In this chapter, we focus on the report's second problem, which is frictional sliding of planar bodies. The relationship between frictional loads and motion is studied, and a simple yet accurate model is proposed. This model is essential because frictional loads can be computed for a given motion direction, but estimating the motion direction for a given frictional load requires solution to some non-linear equations. Since robots may be forced to push objects in a specific direction due to some obstacles or mechanical limitations, these models may be used in the path and motion planning decisions. This force-motion mapping lead to some closed convex surfaces called the limit surface. We formulate a model to approximate these limit surfaces. There have been many studies to approximate these limit surfaces using various methods, a brief overview of which is presented in 3.1. We look at what these limit surfaces are, how to generate them and establish our method to approximate these surfaces and make comparison to the previous work.

3.1 Related work

In this section, we review some literature which is closest to our proposed work . One of the earliest work that presented modeling of limit surfaces was presented in [1]. Our work is mostly inspired from the analysis presented in [1]. In [1], authors show that all possible static and sliding frictional wrenches form a convex set whose boundary is called the limit surface. In [2], authors show that the limit surface can be approximated by a three-dimensional ellipsoid. These ellipsoids are fitted by calculating the maximum friction force and maximum moment, and then used to calculate the major and minor axis as well as the tilt angles of the ellipsoid. This model was proposed in 1996, and was designed to

reduce the computational load required to generate an approximate limit surface. Now with advancements in technology, complex models can be constructed giving more accurate approximations for the limit surfaces.

More recently, [3] presented a framework of representing planar sliding force-motion models using homogeneous even-degree sum-of-squares (sos) convex polynomials. These can be identified by solving a semi-definite program, and the set of applied wrenches can be obtained by 1-sublevel set of a convex polynomial [3].

The work presented in [1] shows an elliptical approximation of the limit surface which is computationally simple to evaluate. Consequently, this model has been widely used for various manipulation tasks [4, 5, 6, 7, 8, 9].

3.2 Analytical model for pusher slider system

Consider the case of a rigid body sliding on a plane. This body's only interaction with the surface is frictional forces. The normal force or pressure at the point of contact or surface is known. The magnitude of frictional force at each location is determined solely by the orientation and direction of slipping of the body, not by the magnitude of slipping. A reference point C is chosen, a unit motion vector $\mathbf{q}$ has the components which are the translation velocity and angular velocity of the reference point $\mathbf{q} = [q_x, q_y, \omega]$.

We chose the reference point as our body's centroid and positioned it at the origin for our convenience. The net frictional load is $\mathbf{P}$=$[F_x, F_y, M]$ where F_x and F_y are the net forces and M is the moment about z axis. These forces can be calculated as integrals over the contact patch. Let $f = [f_{ax}, f_{ay}]$ be the frictional force at a contact point A with coordinates as $r_a = [x_a, y_a]$.

$$F_x = \int_A f_{ax} dx \quad F_y = \int_A f_{ay} dy \quad M = \int_A x_a f_{ax} - y_a f_{ay} dA \tag{3.1}$$

Consider a large number of such motion vectors $\mathbf{q}$ uniformly distributed on the surface of a sphere (we used 2000 such vectors). Using equation 3.1, we can calculate the corresponding $\mathbf{P}$ in load space for each $\mathbf{q}$. In load space, a limit surface can be plotted using this method.

3.3 Limit surfaces and data generation

We shall look at these limit surfaces for some trivial cases. Lets consider an arbitrary body with a single contact point at $(1, 0)$, the calculated the limit surface is plotted in Figure 3.1 in load space.

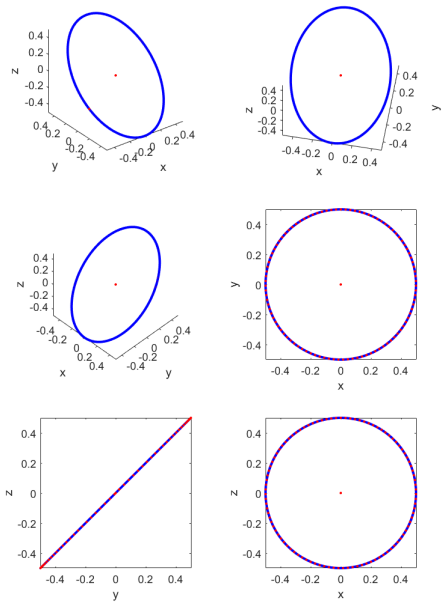

FIGURE 3.1: Limit curve for a single contact point

Consider a two point contact case (a rigid bar with 2 contact point at the ends) as shown in Figure 3.2. The limit surface calculated is plotted in Figure 3.3.

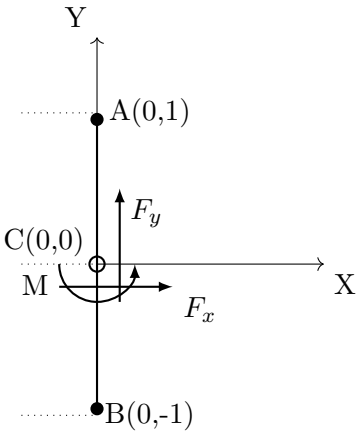

FIGURE 3.2: A rigid bar supported at the ends

Figure 3.3 shows four red circles on the limit curve; these circles form in a specific case when one of the contact points becomes the COR, about which frictional forces cannot be calculated. As long as the frictional force on that contact point is less than the allowable frictional force at that location, the motion will continue. As a result, the surface has flat patches or facets, and it can be concluded that the number of facets on the surface equals two times the number of contact points.

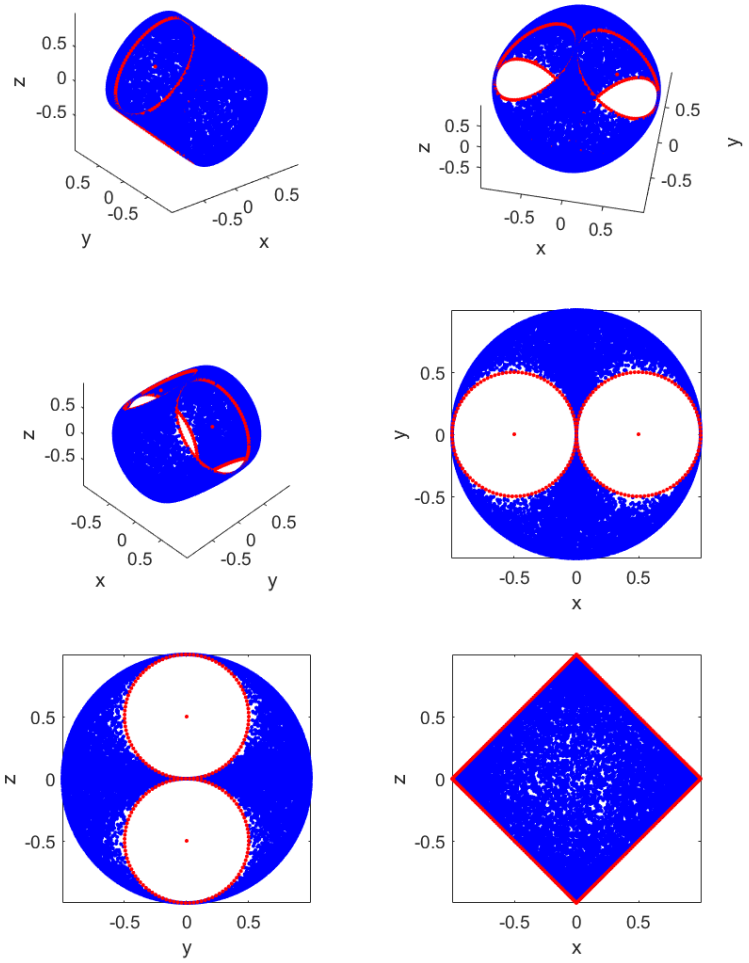

FIGURE 3.3: Limit surface for a rigid bar in Figure(3.2)

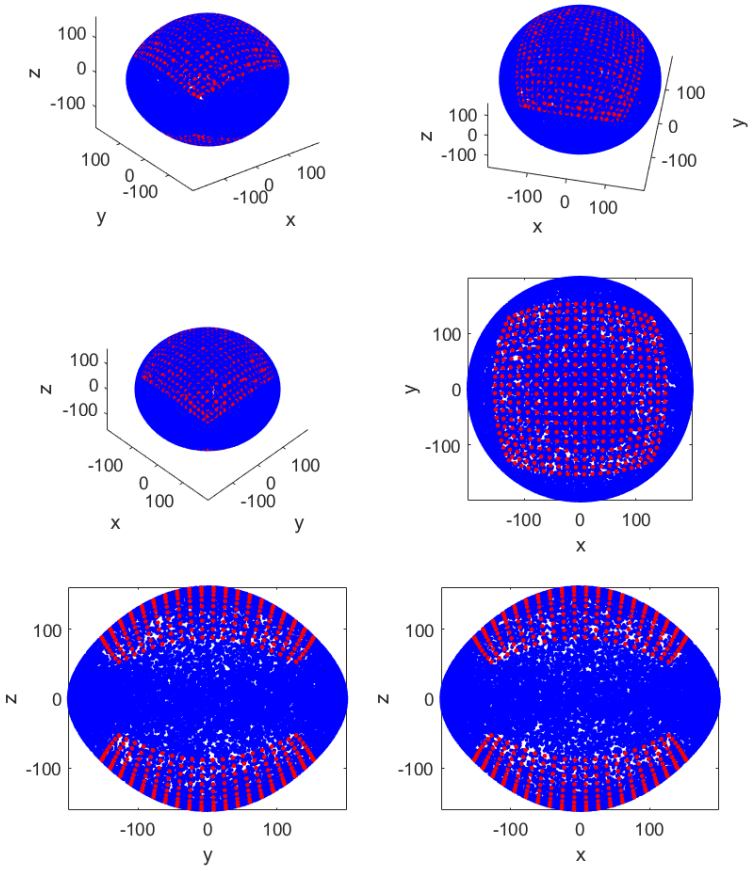

FIGURE 3.4: Limit surface for a continuous square patch

In the case of continuous contact patches (taking 100 uniformly distributed points), these facets contract to small circles, resulting in a continuous limit surface, as seen in Figure 3.4. Figure 3.4 shows the limit surface for a continuous square patch of length 2 and centred at the origin.

This data of P and q can now be utilised as fitting data for our approximation, but it won't offer us good facets estimates because none of our data points are on the facets. To address this problem, we calculate a few additional points, focusing on the facets. we consider each contact point to be a COR, and calculate velocities and forces on the other contact points while uniformly applying random forces ranging from zero to the maximum allowable frictional force in every direction at the COR. We get our fitting data by combining these data points with the original set.

3.4 Approximations

We want to approximate the limit surface as seen in Figures 3.3 and 3.4 such that for every **q** we can find the corresponding **P** and vice versa using our formulation. For the same we define a failure surface $H_i(f)$, subscript i denotes the number of terms in approximation. $H(f) = 1$ implies f lies on the limit surface and the corresponding velocity is given by the normalized unit gradient or the surface normal at that point, $v = \frac{\nabla H(f)}{\|\nabla H(f)\|}$.

$$H_1 = f^T A f \quad \text{1 term app} \tag{3.2}$$

$$H_2 = f^T A f + (f^T B f)^{1/2} \quad \text{2 term app} \tag{3.3}$$

$$H_3 = f^T A f + (f^T B f)^{2/3} + (f^T C f)^{1/3} \quad \text{3 term app} \tag{3.4}$$

We chose the following objective functions to get a fit for the limit surface. We fit out failure surface using two types of objective functions **J1** and **J2**. The following are the objective functions with increase in terms of the approximation. We will consider upto 4 terms in our analysis, the subscript denotes the no of terms in the failure surface.

$$J1_1 = \sum_{k=1}^{n} (f_k^T A f_k - 1)^2 \tag{3.5}$$

$$J2_1 = \sum_{k=1}^{n} (f_k^T A f_k - 1)^2 + \|v_k - \hat{v})\|^2 \tag{3.6}$$

$$J1_2 = \sum_{k=1}^{n} (f_k^T A f_k + (f_k^T B f_k)^{1/2} - 1)^2 \tag{3.7}$$

$$J2_2 = \sum_{k=1}^{n} (f_k^T A f_k + (f_k^T B f_k)^{1/2} - 1)^2 + \|v_k - \hat{v}\|^2 \tag{3.8}$$

$$J1_3 = \sum_{k=1}^{n} (f_k^T A f_k + (f_k^T B f_k)^{2/3} + (f_k^T C f_k)^{1/3} - 1)^2 \tag{3.9}$$

$$J2_3 = \sum_{k=1}^{n} (f_k^T A f_k + (f_k^T B f_k)^{2/3} + (f_k^T C f_k)^{1/3} - 1)^2 + \|v_k - \hat{v}\|^2 \tag{3.10}$$

Here f_k and v_k is are the load and motion vector from the fitting data, $\hat{v}$ is the approximated motion vector and A, B, C are matrices that are found by minimizing the objective function J wrt to parameters in matrices A, B, C using simple optimization strategy. We define A, B, C such that they are symmetrical and positive semi definite, via the cholesky decomposition.

Now that A, B, C are known, let α be some parameter such that αf_k causes slip, i.e:- αf_k resides on the limit surface. Therefore αf_k must follow the following condition-

$$\alpha^2 f_k^T A f_k = 1 \quad \text{1 term app} \tag{3.11}$$

$$\alpha^2 f_k^T A f_k + (\alpha^2 f_k^T B f_k)^{1/2} = 1 \quad \text{2 term app} \tag{3.12}$$

$$\alpha^2 f_k^T A f_k + (\alpha^2 f_k^T B f_k)^{2/3} + (\alpha^2 f_k^T C f_k)^{1/3} = 1 \quad \text{3 term app} \tag{3.13}$$

The above equations are simple polynomial equations in α and can be easily solved. With the aforementioned method we can construct the limit surface, moreover we can determine forces that cause slip in any arbitrary direction by considering a unit vector in that direction and scaling it such that it lies on the limit surface.

We study our approximation for two particular cases. First for a right angled triangle with contact points at the each of the vertices and second for the same triangle but with a continuous contact patch. The reference point C is taken as the centroid of the triangle and positioned at the origin. The limit surfaces constructed are plotted in Figures 3.5 and 3.6.

Figure 3.5 illustrates the fitting data set and the approximated surface. In Figure 3.5a it can be observed that as the terms in approximation increase the features of the facets are captured effectively. 1 term approximation which is basically an ellipsoid approximation struggles to capture the facets whereas 3 term approximation is able to capture these features. Figure 3.5b shows the results of adding an extra velocity error in our objective function, the corresponding failure surface may not be as accurate as in Figure 3.5a but, should give us better velocity approximations as compared to **J1**. This is further studied in the next section.

Figure 3.6 shows the fitting data and the approximated surface for the continuous contact patch. It can be seen that the 1 term approximation does not perform well, as it maps most of the data set to the center of the surface. Higher terms of J1 and J2 fits the surface well.

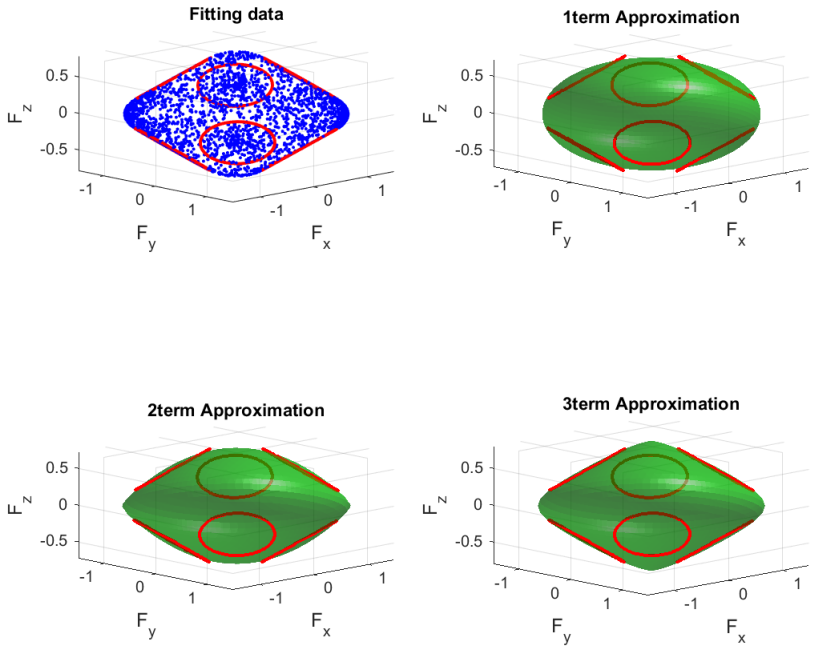

(A) Approximations using J1

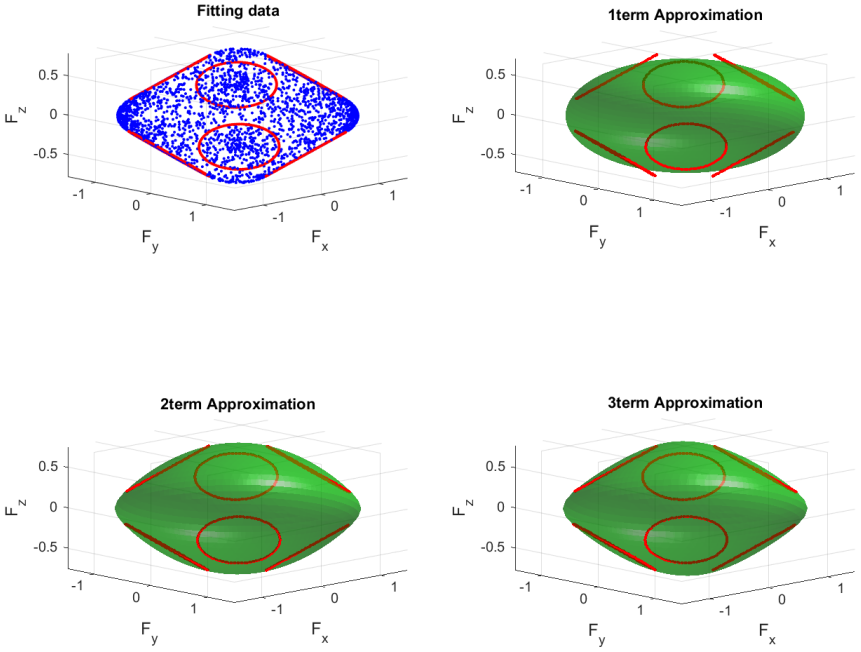

(B) Approximations using J2

FIGURE 3.5: Approximated LS for 3 point contact

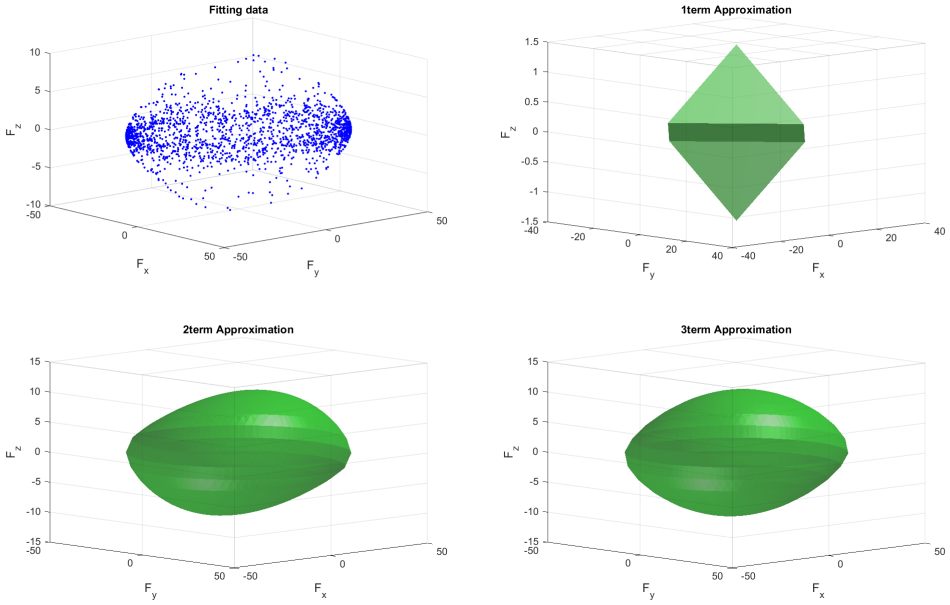

(A) Approximations using J1

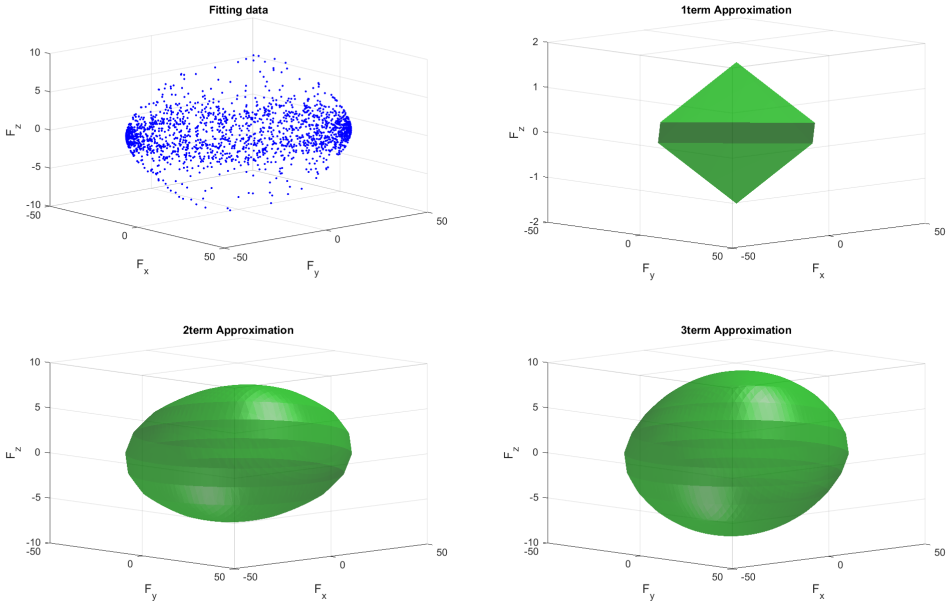

(B) Approximations using J2

FIGURE 3.6: Approximated LS for continuous patch

We try another method to optimize the 2 term approximation with the same objective function, but here we minimize the objective function wrt B. Lets call this second approximation and note that A is only symmetrical while B is symmetrical and positive semi definite. A is solved in a least square sense using the eqn(3.14) and the objective function is minimized wrt parameters in matrix B.

$$f_k^T A f_k = 1 - (f_k^T B f_k)^m \tag{3.14}$$

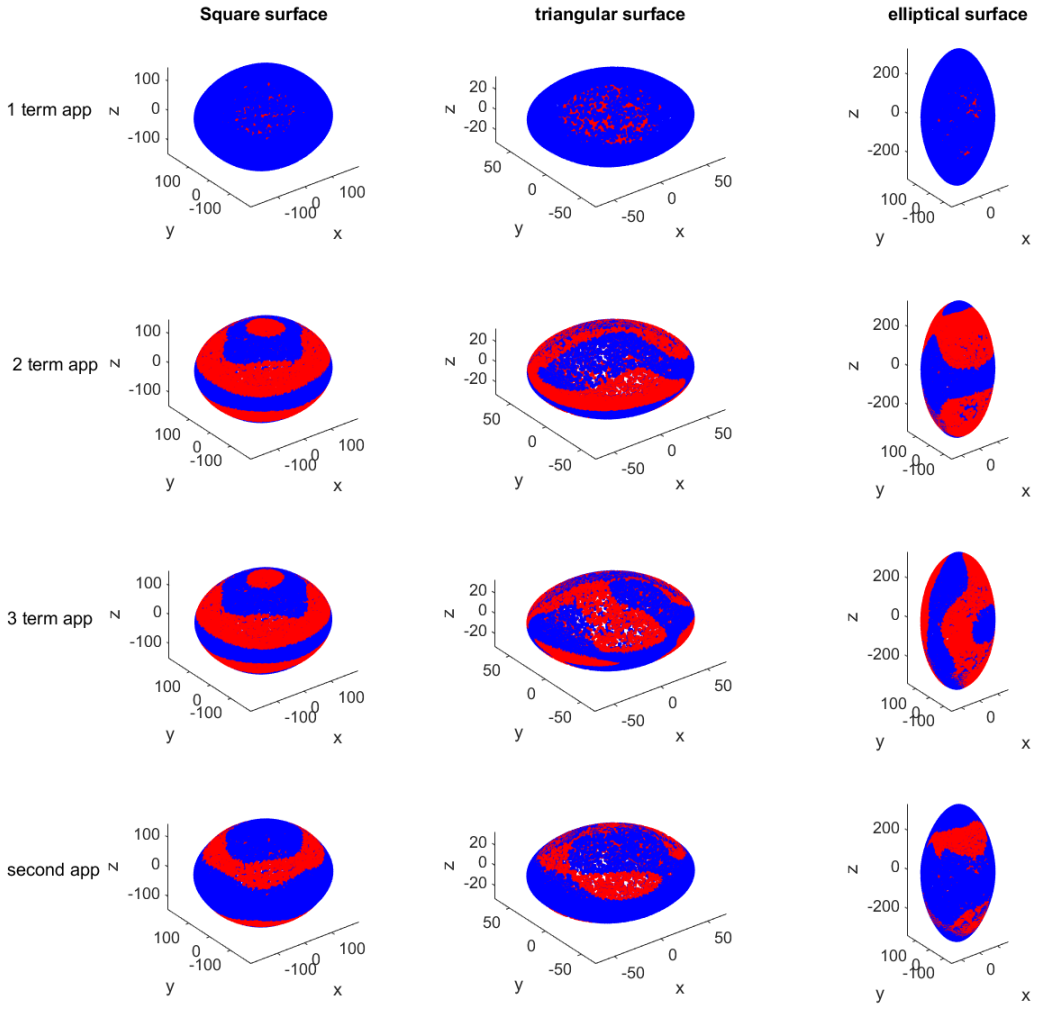

FIGURE 3.7: Approximations: blue- original red- approximation

Figure 3.7 shows upto three term approximation of limit surfaces for three different continuous surfaces, square, triangular and elliptical. The blue surface is the original data and the red surface is the approximated surface. It is clear that the 1 term approximation (ellipsoidal approximation) struggles, whereas the higher term approximations perform better.

3.5 Error measure

To study how the approximation performs with increase in terms, two types of error measure are defined, force based and velocity based. In velocity based error, for a testing data (f, v), velocity $\hat{v}$ is calculated using normalised surface normal given by the gradient, $\hat{v} = \frac{\nabla H(f)}{\|\nabla H(f)\|}$ and error is defined as the norm of the difference between the two $\|v - \hat{v}\|$. Since v and $\hat{v}$ are unit vectors, error can range from zero to two.

In force based error, 1000 unit vectors lying uniformly on the surface of the sphere are considered, which are then scaled using equations 3.11, 3.12, such that they lie on LS. Lets call them f_s (scaled force), using f_s velocity $\hat{v}$ is calculated. Now using $\hat{v}$, corresponding forces $\hat{f}$ are calculated by equation 3.1. Force error is defined as the norm of the difference between f_s and $\hat{f}$ $\|f - \hat{f}\|$.

The empirical distribution of the errors are plotted in Figures 3.8 and 3.9 to compare the different fits and objective functions. A fourth order convex polynomial fit as described in [3] is also superimposed on the plots for comparison.

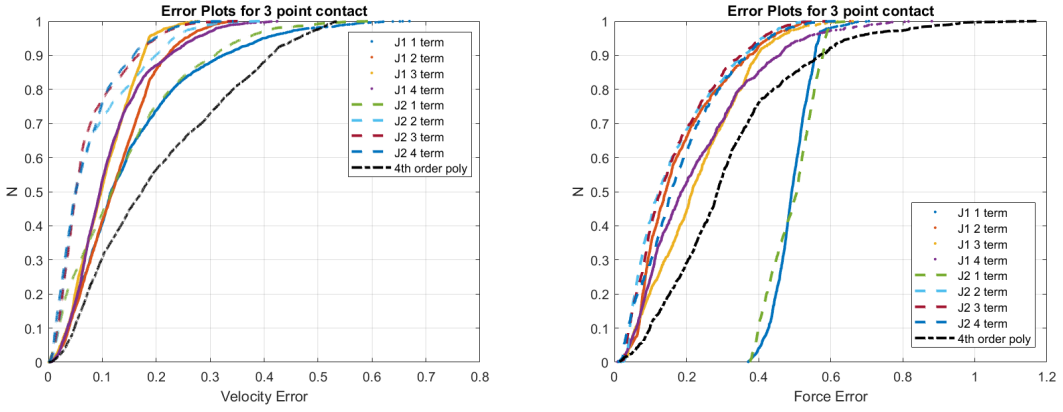

(A) Velocity error distribution (B) Force error distribution

FIGURE 3.8: Error plots for 3 point contact

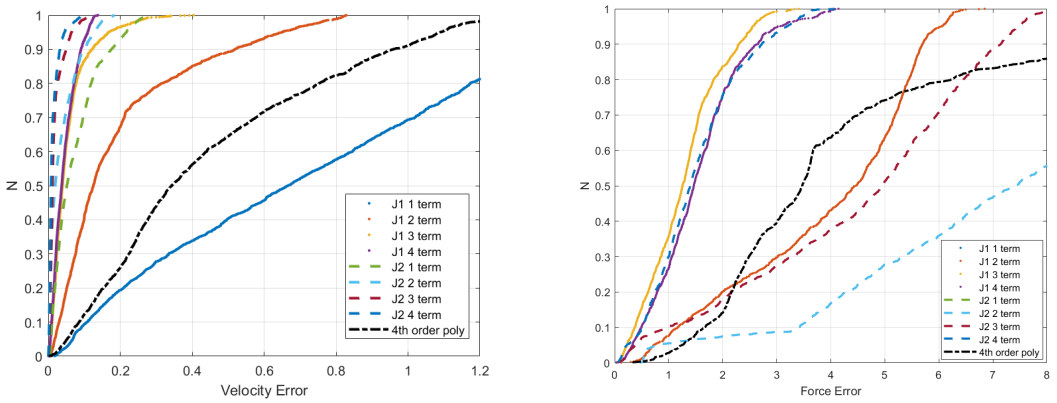

(A) Velocity error distribution

(B) Force error distribution

FIGURE 3.9: Error plots for continuous distribution

In velocity error distributions, J2 performs better than J1 as expected and with higher terms performance of the approximation increases (100% of the points have errors less than 0.3). Almost every approximation performs better than the fourth order polynomial in case of 3 point contact. Same observations can be drawn in case of continuous contact patch except that fourth order polynomial performs better that J1 1 term approximation which is basically an ellipsoid.

In force error distributions, J2 higher terms perform similar to J1 2 term. We observe that 1 term approximations perform poorly in case of 3 point contact which is expected since they are ellipsoidal approximation and wont be able to capture the features of the facets. In case of 3 point contact, higher order approximation perform much better than the fourth order polynomial. And in case of continuous contact patch J1 perform much better than J2, as J1 is designed to fit the failure surface. Higher terms of J1 and J2 both perform better than the fourth order polynomial.

To test the robustness of our formulation we add noise to the training as well as testing data and repeat the above process to verify the results. With noise introduced in the data the results don't vary drastically as seen in Figures 3.10 and 3.11. But a change can be noticed in velocity error plot for the continuous case (Figure 3.11a), With the noise introduced in the system J1 and J2 perform equally contrary to Figure 3.9a, where J2 outperformed J1 suggesting it might be over fitting the velocity data. It can be taken care of by introducing a multiplication factor in the velocity error term in J2.

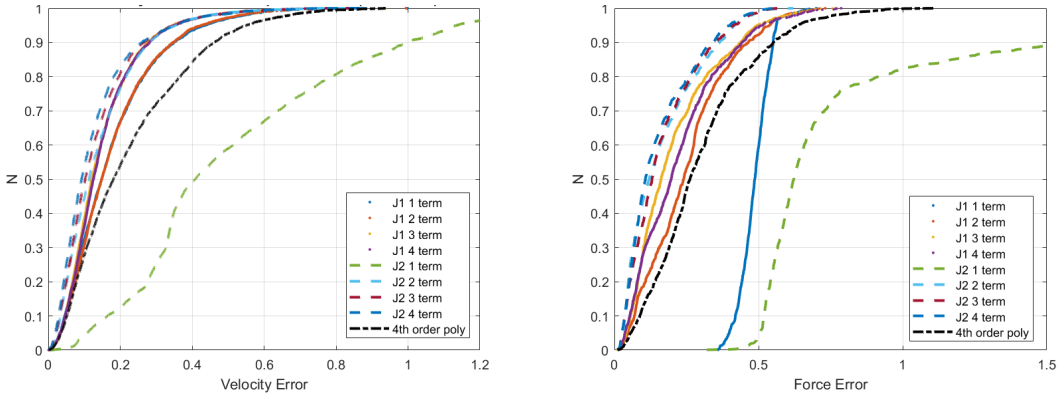

(A) Velocity error distribution (B) Force error distribution

FIGURE 3.10: Error plots for 3 point contact with noisy data

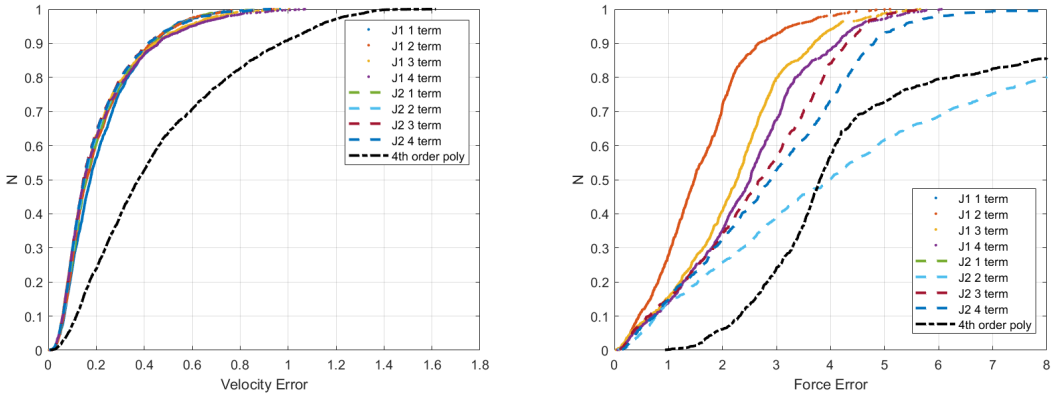

(A) Velocity error distribution (B) Force error distribution

FIGURE 3.11: Error plots for continuous contact patch with noisy data

Chapter 4

Conclusions

With concluding remarks and future scope of study, we outline our work on both areas.

4.1 Decaying functions

4.1.1 Concluding remarks

We devised a method to approximate a system's decaying response as a sum of exponentials. We construct a DDE and utilise its roots as a basis for approximating the functions. With a small number of terms in the approximation, the fit is similar but oscillates, but with a high number of terms in the approximation, the fit is excellent with very small amplitude oscillations which is reflected in the error plots. We evaluated the method for some more decaying functions. The method gave a poor fit with a function that changes slope mid-way (function 3 in Figure 2.8).

4.1.2 Future scope

In the proposed method, there are a few more aspects to look into. We used integrals to build our DDE, but what other forms of equations may work can be investigated. To discover and approximate f, we employ an ad hoc method that must be addressed individually for each function. It remains to be seen whether an analytic solution for f can be found. Better optimization methods can be utilised once a basis are obtained.

4.2 Limit surfaces

4.2.1 Concluding remarks

We gave a quick introduction of limit surfaces, their importance and previous research into them. In the past, approximations for these limit surfaces have included ellipsoids in the simplest case, and multivariate polynomial expansions, a more sophisticated example. We proposed a new approximation which uses a small number of symmetrical 3×3 matrices along with fractional powers of simple quadratic forms. We fit our matrices using different techniques, concluding that there is a trade-off between load and motion predictions when determining the objective function. One (J2) would provide a better motion approximation, whereas the other (J1) would better fit the limit surface. We evaluated our formulation in a few scenarios and plotted errors, noting that higher term approximations are better than the commonly used ellipsoidal approximation and also outperforms the more complex fourth order convex polynomial fit.

4.2.2 Future scope

This study's analysis was based on theoretical data. It remains to be seen how the formulation performs when tested against various experimental data sets. Because multiple local minima were discovered while fitting the matrices, more sophisticated optimization procedures may result in superior fits.

Appendix A

Matlab codes

A.1 Approximation for decaying functions

A.1.1 Finding delay feedback

```
function f=findf(t,x)
dt=t(2)-t(1);
xd=[x(2:end)-x(1:end-1);0]/dt;
n=length(x);
A=zeros(n);
for k=1:n
    f=zeros(n,1);
    f(k)=1;
    c=conv(x,f);
    A(:,k)=c(1:n)*dt;
end
f=A\xd;
end
```

A.1.2 Infinity norm solver

```
function x=inf_norm_sol(A,b)
% solves Ax=b approximately such that Ax-b is minimized in the
% infinite-norm as opposed to x=A\b, which minimizes Ax-b in the 2-norm.
% It is assumed that A has n rows and m columns, with n >= m,
% and that b has n rows and ONE column
[n,m]=size(A);
```

```
f=[1;zeros(n+m,1)];
% op=optimset('maxiter',2000) this is an optional command
AA=[zeros(n,1),-eye(n),A];
B=zeros(2*n+1,n+m+1);
B(:,1)=-ones(2*n+1,1);
B(2:n+1,2:n+1)=eye(n);
B(n+2:2*n+1,2:n+1)=-eye(n);
z=zeros(2*n+1,1);
% x=linprog(f,B,z,AA,b,[],[],[],op); % use this, in place of the
% following line, if options are set above
x=linprog(f,B,z,AA,b);
x=x(n+2:end);
end
```

A.2 Approximation for limit surface

A.2.1 Data generation

```
function [F,v]=datagen
%% normal generated
num=2000;
n=randn(num,3);
for i=1:num
    n(i,:)=n(i,:)/norm(n(i,:));
end
v=n;
%% forces generated
r=[[-40,-40,0];[-40,80,0];[80,-40,0]]; % vertices of the triangle
r=r/150;
[m1,m2]=size(r);
mu=(0.5)*ones(m1); % friction distribution
for j=1:num
    for i=1:m1
        vk(i,:)=n(j,:)+cross([0,0,n(j,3)],r(i,:)); % calculating velocity of each vertex
        f(i,:)=mu(i)*vk(i,1:2)/norm(vk(i,1:2));    % calculating fx and fy
        mk(i,:)=cross(r(i,:),[f(i,:),0]);           % calculating moment
    end
    F(j,:)=[sum(f(1:end,:)),sum(mk(1:end,end))];
end
v1=[];
% to calculate data for facets
for j=1:m1
```

```
    rc=r(j,:);          % position of COR
    omega=1;
    n1=cross([0,0,omega],-rc); % velocity of reference point
    n1(3)=omega;
    n1=n1/norm(n1);
    for i=1:length(r(:,1))
        vk(i,:)=-cross(r(i,:)-rc,[0,0,omega]); % Velocity at vertices
        if rc==r(i,:)       % force at COR is taken 0, will be adding random values in
    ↪ next section
            f(i,:)=[0,0];
            mk(i,:)=cross(r(i,:),[f(i,:),0]);
        else
            f(i,:)=mu(i)*vk(i,1:2)/norm(vk(i,1:2)); % forces at other vertices
            mk(i,:)=cross(r(i,:),[f(i,:),0]);
        end
    end
    F1(j,:)=[sum(f(1:end,:)),sum(mk(1:end,end))]; % total force
    v1=[v1;n1]; % respective velocity
end
F2=-F1; % to account for clockwise and anticlockwise
v2=-v1;
ff=[];
vv=[];
cnt=150;    % no of data points on the facets
theta=linspace(0,2*pi,cnt); % will be adding force at COR in all directions
for i=1:m1
    for j=1:cnt
        t=rand/2;   % friction distribution at COR (anything less than muN )
        f1=t*[sin(theta(j)),cos(theta(j))];
        mk(i,:)=cross(r(i,:),[f1,0]);
        f=[f1,mk(i,3)]+F1(i,:); % adding force at cor to the total force
        ff=[ff;f];
        %plot3(f(1,1),f(1,2),f(1,3),'.r')
        vv=[vv;v1(i,:)];    % accounting for corresponding velocity
    end
    % same process below when direction of rotation is reversed
    for j=1:cnt
        t=rand/2;
        f1=t*[sin(theta(j)),cos(theta(j))];
        mk(i,:)=cross(r(i,:),[f1,0]);
        f=[f1,mk(i,3)]+F2(i,:);
        ff=[ff;f];
        %plot3(f(1,1),f(1,2),f(1,3),'.r')
        vv=[vv;v2(i,:)];
    end
```

```
end
v=[v;vv]; %
F=[F;ff];
```

A.2.2 Velocity error

```
function [Ev]=getappV(q)
t=q(1:6);
A=[[t(1);0;0],[t(2:3);0],[t(4:6)]];
A=A'*A;
if length(q)>6
    t=q(7:12);
end
B=[[t(1);0;0],[t(2:3);0],[t(4:6)]];
B=B'*B;
if length(q)>12
    t=q(13:18);
end
C=[[t(1);0;0],[t(2:3);0],[t(4:6)]];
C=C'*C;
if length(q)>18
    t=q(19:24);
end
D=[[t(1);0;0],[t(2:3);0],[t(4:6)]];
D=D'*D;
E=0;
Ev=[];
load FV_test_noise
[n1,n2]=size(F);
Fapp=[];
vapp=[];
for k=1:n1
    f=F(k,:);
    va=v(k,:);
    if length(q)==6
        g=2*f*A;
        g=g/norm(g);
        vapp=[vapp;g];
        Ev=[Ev;norm(va-g)];

    elseif length(q)==12
        g=2*f*A+(1/2)*((f*B*f')^(-1/2))*(2*f*B);
        g=g/norm(g);
```

```
        vapp=[vapp;g];
        Ev=[Ev;norm(va-g)];

    elseif length(q)==18
        g=2*f*A+(1/3)*((f*B*f')^(-2/3))*(2*f*B)+(2/3)*((f*C*f')^(-1/3))*(2*f*C);
        g=g/norm(g);
        vapp=[vapp;g];
        Ev=[Ev;norm(va-g)];

    elseif length(q)==24

        g=2*f*A+(1/4)*((f*B*f')^(-3/4))*(2*f*B)+(2/4)*((f*C*f')^(-2/4))*(2*f*C)+(3/4)*((f*
    ↪ D*f')^(-1/4))*(2*f*D);
        g=g/norm(g);
        vapp=[vapp;g];
        Ev=[Ev;norm(va-g)];
    end

end
Ev=sort(Ev);
end
```

A.2.3 Force approximation and error

```
function [Fapp,vapp]=getappF(q)
t=q(1:6);
A=[[t(1);0;0],[t(2:3);0],[t(4:6)]];
A=A'*A;
if length(q)>6
    t=q(7:12);
end
B=[[t(1);0;0],[t(2:3);0],[t(4:6)]];
B=B'*B;
if length(q)>12
    t=q(13:18);
end
C=[[t(1);0;0],[t(2:3);0],[t(4:6)]];
C=C'*C;
if length(q)>18
    t=q(19:24);
end
D=[[t(1);0;0],[t(2:3);0],[t(4:6)]];
D=D'*D;
```

```
E=0;
Ev=[];
load Fsphere
[n1,n2]=size(F);
Fapp=[];
vapp=[];
for k=1:n1
    f=F(k,:);
    if length(q)==6
        m=0;
        E=E+(f*A*f'-1)^2;
        alpha=(1/(f*A*f'))^1/2;
        if any(imag(alpha))
            disp(alpha);
            error('alpha is imaginary')
        end

        Fapp=[Fapp;alpha*f];
        f=alpha*f;
        g=2*f*A;
        g=g/norm(g);
        vapp=[vapp;g];

    elseif length(q)==12
        m1=0.5;
        E=E+(f*A*f'+(f*B*f')^m1 -1)^2;
        c=roots([f*A*f',(f*B*f')^m1,-1]);
        cr=c(imag(c)==0);
        cr=cr(real(cr)>=0);
        cc=abs(cr-1);
        [m,n]=min(cr);
        alpha=cr(n);
        if any(imag(alpha))
            disp(alpha);
            disp(cr(n));
            disp(cr);
            error('alpha is imaginary')
        end
        Fapp=[Fapp;alpha*f];

        f=alpha*f;
        g=2*f*A+(1/2)*((f*B*f')^(-1/2))*(2*f*B);
        g=g/norm(g);
        vapp=[vapp;g];

```

```
65
66      elseif length(q)==18
67          m1=1/3; m2=2/3;
68          E=E+(f*A*f'+(f*B*f')^m1+(f*C*f')^m2 -1)^2;
69          c=roots([f*A*f',(f*C*f')^m2,(f*B*f')^m1,-1]);
70          cr=c(imag(c)==0);
71          cr=cr(real(cr)>=0);
72          cc=abs(cr-1);
73          [m,n]=min(cr);
74          alpha=(cr(n))^(3/2);
75          if any(imag(alpha))
76              disp(alpha);
77              disp(cr(n));
78              disp(cr);
79              error('alpha is imaginary')
80          end
81          Fapp=[Fapp;alpha*f];
82
83          f=alpha*f;
84          g=2*f*A+(1/3)*((f*B*f')^(-2/3))*(2*f*B)+(2/3)*((f*C*f')^(-1/3))*(2*f*C);
85          g=g/norm(g);
86          vapp=[vapp;g];
87
88
89      elseif length(q)==24
90          m1=1/4; m2=2/4; m3=3/4;
91          E=E+(f*A*f'+(f*B*f')^m1+(f*C*f')^m2 +(f*D*f')^m3 -1)^2;
92          c=roots([f*A*f',(f*D*f')^m3,(f*C*f')^m2,(f*B*f')^m1,-1]);
93          cr=c(imag(c)==0);
94          cr=cr(real(cr)>=0);
95          cc=abs(cr-1);
96          [m,n]=min(cr);
97          alpha=(cr(n))^(2);
98          if any(imag(alpha))
99              disp(alpha);
100             disp(cr(n));
101             disp(cr);
102             error('alpha is imaginary')
103         end
104         Fapp=[Fapp;alpha*f];
105
106         f=alpha*f;
107         g=2*f*A+(1/4)*((f*B*f')^(-3/4))*(2*f*B)+(2/4)*((f*C*f')^(-2/4))*(2*f*C)+(3/4)*((f*
    ↪ D*f')^(-1/4))*(2*f*D);
108         g=g/norm(g);
```

```
        vapp=[vapp;g];
    end

end
```

```
function [EF]=F_error
load fvn_j2_1term % contains Fapp and vapp generated from above code
[num,num1]=size(Fa);
n=va;
%% forces generated
%r=[[0,1,0];[cosd(30),-sind(30),0];[-cosd(30),-sind(30),0]];
r=[[-40,-40,0];[-40,80,0];[80,-40,0]];
r=r/150;
[m1,m2]=size(r);
mu=(0.5)*ones(m1);
EF=[];
EFr=[];
for j=1:num
    for i=1:m1
        vk(i,:)=n(j,:)+cross([0,0,n(j,3)],r(i,:));
        f(i,:)=mu(i)*vk(i,1:2)/norm(vk(i,1:2));
        mk(i,:)=cross(r(i,:),[f(i,:),0]);
    end
    F(j,:)=[sum(f(1:end,:)),sum(mk(1:end,end))];
    EF=[EF;norm(F(j,:)-Fa(j,:))];
end
v=n;
EF=sort(EF);
end
```

Bibliography

[1] S. Goyal, A. Ruina, and J. Papadopoulos, "Planar sliding with dry friction part 1. limit surface and moment function," *Wear*, vol. 143, no. 2, pp. 307–330, 1991.

[2] R. D. Howe and M. R. Cutkosky, "Practical force-motion models for sliding manipulation," *The International Journal of Robotics Research*, vol. 15, no. 6, pp. 557–572, 1996.

[3] J. Zhou, R. Paolini, J. A. Bagnell, and M. T. Mason, "A convex polynomial force-motion model for planar sliding: Identification and application," in *2016 IEEE International Conference on Robotics and Automation (ICRA)*, 2016, pp. 372–377.

[4] K. M. Lynch and M. T. Mason, "Stable pushing: Mechanics, controllability, and planning," *The international journal of robotics research*, vol. 15, no. 6, pp. 533–556, 1996.

[5] M. R. Dogar and S. S. Srinivasa, "Push-grasping with dexterous hands: Mechanics and a method," in *2010 IEEE/RSJ International Conference on Intelligent Robots and Systems*. IEEE, 2010, pp. 2123–2130.

[6] N. C. Dafle, A. Rodriguez, R. Paolini, B. Tang, S. S. Srinivasa, M. Erdmann, M. T. Mason, I. Lundberg, H. Staab, and T. Fuhlbrigge, "Extrinsic dexterity: In-hand manipulation with external forces," in *2014 IEEE International Conference on Robotics and Automation (ICRA)*. IEEE, 2014, pp. 1578–1585.

[7] K. Yu, M. Bauza, N. Fazeli, and A. Rodriguez, "More than a million ways to be pushed. a high-fidelity experimental dataset of planar pushing," in *2016 IEEE/RSJ international conference on intelligent robots and systems (IROS)*. IEEE, 2016, pp. 30–37.

[8] W. Zhang, S. Seto, and D. K. Jha, "Cazsl: Zero-shot regression for pushing models by generalizing through context," 2020.

[9] N. Chavan-Dafle and A. Rodriguez, "Prehensile pushing: In-hand manipulation with push-primitives," in *2015 IEEE/RSJ International Conference on Intelligent Robots and Systems (IROS)*. IEEE, 2015, pp. 6215–6222.